Int. J. Multiphase Flow Vol. 9, No. 2, pp. 203–217, 1983
Printed in Great Britain.

0301-9322/83/020203-15$03.00/0
Pergamon/Elsevier

PATHLINES AROUND FREELY ROTATING SPHEROIDS IN SIMPLE SHEAR FLOW

Z. ADAMCZYK and T. G. M. VAN DE VEN

Pulp and Paper Research Institute of Canada and Department of Chemistry, McGill University, Montreal, Quebec, Canada, H3A 2A7

(*Received* 20 *April* 1982; *in revised form* 29 *June* 1982)

Abstract—The pathlines around oblate and prolate spheroids freely rotating in shear flow according to Jeffery's equations have been calculated numerically. When the spheroid is aligned with the vorticity axis, open and closed pathlines exist separated by a surface of limiting pathlines. This is very similar to pathlines around spheres and similarly aligned (infinite) cylinders. For spheroids with an arbitrary orientation, four kinds of pathline exist: (i) closed pathlines: (ii) open (single pass) pathlines; (iii) transient orbits; and (iv) permanent non-closed orbits. In general the permanent (closed and non-closed) orbits are separated from the open pathlines by a region occupied by transient orbits.

The relevance of pathlines around spheroids to problems of heat and mass transfer and particle deposition in flowing sols is discussed.

1. INTRODUCTION

Motion of small particles in the neighborhood of larger ones occurs in a variety of systems relevant to industry and medical sciences. Examples are the motion of fillers and fines particles near pulp fibers in papermaking, the motion of mineral fines near air bubbles in flotation and the motion of platelets near erythrocytes in bloodflow. Most of the theoretical literature on the motion and interactions between particles in flowing systems deals with spherical particles because they are relatively easy to treat mathematically. Often, in real systems, particles have shapes which may differ appreciably from spherical ones and it is of interest to know what effect the shape of particles has on particle hydrodynamic interactions, especially with respect to orthokinetic coagulation.

The behavior of two sphere interactions in simple shear flow is now well understood, both in the presence and absence of colloidal interparticle forces. For details the reader is referred to a recent review by van de Ven (1981). The motion of two spheres in shear flow is known for any radius ratio q of the two spheres; when $q = 0$ and the size of one sphere is negligible with respect to the other, the problem reduces to that of finding the streamlines around a single sphere, a problem solved by Cox *et al.* (1968); When $q = 1$ both spheres have equal size and the motion of the spheres is described by a variety of workers (see Arp & Mason 1977, Batchelor & Green 1972). Qualitatively, the trajectories of spheres around a central reference sphere are very similar to the streamlines around a sphere for all values of q. The main difference between the trajectories of various size spheres is the distance of closest approach of two particles on a limiting trajectory in the equatorial plane, i.e. a trajectory which separates the open, separating trajectories, from the closed ones. From the data presented by Adler (1981), it can be shown that for $q < 0.1$ trajectories of spheres differ from streamlines by less than a few percent. Hence the motion of small particles can conveniently be described by streamlines (or for non-steady flows more generally by pathlines) without too much error.

In order to investigate the effect of particle shape on the motion of particles in shear flow, we studied the pathlines around oblate (disk-like) and prolate (rod-like) spheroids freely rotating in a simple shear flow. Analogous to the motion of spheres it is to be expected that such pathlines also accurately describe the trajectories of particles of diameter smaller than about 10% of the minor axis of the spheroid. Furthermore it is to be expected that the motion of larger particles will be qualitatively very similar and thus the description of such pathlines provides a framework for speculating about such motions as well.

The flow around a spheroid with a specified (arbitrary) orientation in a simple shear flow has been given by Jeffery (1922). In this paper we will show how, from Jeffery's solution, the pathlines (or trajectories of small particles) around freely rotating spheroids can be found and present numerical solutions of the equations. In the limiting cases of a sphere (axis ratio $r_p \to 1$) and an infinite cylinder ($r_p \to \infty$) aligned along the vorticity axis, our solutions agree with those given by Cox *et al.* (1968).

2. THEORY

The problem of finding the flow field near an ellipsoid arbitrarily oriented in a simple shear flow of gradient G has been given by Jeffery (1922). For a spheroid with major semi-axis a and minor semi-axes b we will denote the velocity components in particle fixed coordinates $x_i (i = 1, 2, 3)$ by

$$u_i^J = \mathrm{d}x_i/\mathrm{d}t^*, \qquad [1]$$

with $t^* = Gt$, G being the rate of shear and t the time. The axis X_1 is chosen to coincide with the symmetry axis of the spheroids. Expressions for u_i^J can be obtained from Jeffery's equations (22)–(24) by setting $c = b$. Complete expressions are given in the appendix. The particle-fixed coordinates x_i can be transformed in space-fixed coordinates x_i' by means of the matrix α_{ij}:

$$x_i' = \alpha_{ij} x_j \qquad [2]$$

(where the summation convention for repeated indices is used), where α_{ij} is given by

$$\alpha_{ij} = \begin{pmatrix} \cos\theta & -\sin\theta\cos\psi & -\sin\theta\sin\psi \\ \sin\theta\cos\phi & -\sin\phi\sin\psi + \cos\theta\cos\phi\cos\psi & -\sin\phi\cos\psi - \cos\theta\cos\phi\sin\psi \\ \sin\theta\sin\phi & \cos\phi\sin\psi + \cos\theta\sin\phi\cos\psi & \cos\phi\cos\psi - \cos\theta\sin\phi\sin\psi \end{pmatrix}. \qquad [3]$$

Here the angles ϕ, θ and ψ are Euler's angles (see figure 1) specifying the orientation of the spheroid with respect to the space fixed Cartesian coordinates x_i'.

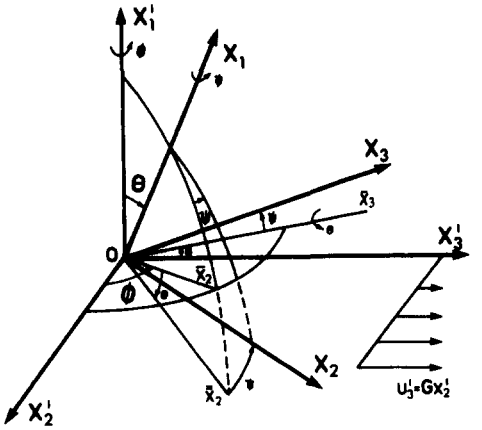

Figure 1. Particle fixed coordinate system X_i relative to space fixed coordinate system X_i'. The axis of revolution of the spheroid coincides with the X_1-axis. The orientation of the spheroid can be described by the Euler angles ϕ, θ, ψ, defined in the following way: (i) rotate space fixed coordinates around X_1' by an angle ϕ to yield X_1', $\bar{x}_2$, $\bar{x}_3$; (ii) rotate X_1', $\bar{X}_2$, $\bar{x}_3$ around $\bar{x}_3$ by an angle θ to yield X_1, $\bar{x}_2$, $\bar{x}_3$; (iii) rotate X_1, x_2 $\bar{x}_3$ around X_1 by an angle ψ to obtain X_1, X_2, X_3.

The motion of the spheroid in simple shear is described by the following set of equations (Jeffery 1922):

$$\frac{d\theta}{dt^*} = \frac{1}{4} B \sin 2\theta \sin 2\theta \qquad [4a]$$

$$\frac{d\phi}{dt^*} = \frac{1}{2}(1 + B \cos 2\phi) \qquad [4b]$$

$$\frac{d\psi}{dt^*} = -\frac{1}{2} B \cos\theta \cos 2\phi \qquad [4c]$$

where $B = (r_p^2 - 1)/(r_p^2 + 1)$, r_p being the particle axis ratio a/b.

In a time interval Δt^* an element of fluid (or a small particle with radius $\ll b$) moves by an amount $u^J \Delta t^*$ with respect to the spheroid with orientation (θ, ϕ, ψ). In the same time interval the spheroid rotates by an amount $\Delta\theta, \Delta\phi, \Delta\psi$. To obtain the coordinates with respect to particle fixed axes which rotate along with the spheroid, the new position of the fluid element must be expressed in terms of this rotating coordinate system. This can be achieved by two simultaneous transformations, first by transforming the position into space fixed coordinate using α_{ij} evaluated at time t^* and subsequently transforming the space fixed coordinates into rotating particle fixed coordinates using α_{ji} evaluated at $t^* + \Delta t^*$. As a result the motion of a fluid element (material point) with respect to particle fixed coordinates rotating according to Jeffery's equations is given by:

$$u_i = u_i^J + \beta_{ij} x_j, \qquad [5]$$

where

$$\beta_{kl} = \alpha_{jl} \dot{\alpha}_{jk}, \qquad [6]$$

and where the dot denotes differentiation with respect to the time, i.e. $\dot{\alpha}_{ij} = d\alpha_{ij}/dt^*$. The components of $\dot{\alpha}_{ij}$ can be found from [3] and [4].

Alternatively the transformation from particle fixed coordinates when the spheroid is fixed in space to particle fixed coordinates when the spheroid is free to rotate can be expressed as (see e.g. Batchelor 1976):

$$\mathbf{u} = \mathbf{u}^J - \boldsymbol{\omega} \times \mathbf{x} \qquad [7]$$

which is identical to [5] with β_{ij} given by

$$\beta_{ij} = \begin{pmatrix} 0 & \omega_3 & -\omega_2 \\ -\omega_3 & 0 & \omega_1 \\ \omega_2 & -\omega_1 & 0 \end{pmatrix} \qquad [8]$$

where the ω_i's are the spins around the three axes of the spheroid given by

$$\omega_1 = \frac{1}{2}\cos\theta$$

$$\omega_2 = \sin\psi \frac{d\theta}{dt^*} - \sin\theta \cos\psi \frac{d\phi}{dt^*}$$

$$\omega_3 = \cos\psi \frac{d\theta}{dt^*} + \sin\theta \sin\psi \frac{d\phi}{dt^*}.$$

It can readily be shown that [6] and [8] are equivalent.

It should be noted that x_i in [1] are the coordinates associated with the fixed position of the spheroid while in [5] they specify the position in particle fixed coordinates rotating along with the spheroid.

The solution of [5] yields the pathlines around freely rotating spheroids in particle fixed coordinates. Using [2] the solution can be transformed into space fixed coordinates:

$$x_i'(t^*) = \alpha_{ij}(t^*)x_j(t^*). \qquad [9]$$

The problem of finding the pathlines around rotating spheroids thus reduces itself to solving [5] numerically and transforming the solution into space fixed coordinates using [9]. Results of such calculations are presented in the next section. The set of equations [5] together with [4] yields a set of six coupled differential equations. Equations [4a] and [4b] can be integrated analytically, while [4c] gives rise to an elliptic integral. We found it convenient to integrate [4c] together with [5] resulting in a set of four coupled differential equations which were integrated numerically using a Runge Kutta method. Results for $r_p = 1$ and $r_p = \infty$ (i.e. > 100) were checked by comparison with exact solutions given by Cox *et al.* (1968).

3. RESULTS AND DISCUSSION

(a) *Spheroids aligned along the vorticity axis*

When the spheroid is aligned with the vorticity axis X_1', i.e. when $\theta = 0°$, the pathlines are very similar to those around spheres and cylinders described by Cox *et al.* (1968). In this case two kinds of pathline exist, closed ones and open ones, separated by a surface of limiting pathlines. Such pathlines are shown schematically in figure 2. We define $d^*_{min} = d_{min}/b$ as the dimensionless minimum distance between the pathline and the surface of the spheroid for a given closed orbit (in whatever plane) and d^*_{max} the corresponding dimensionless maximum distance. Results of values of d^*_{min} and d^*_{max} for various axis ratio's r_p, calculated from [5] and [6] are shown in figure 3 for orbits in the $X_2'X_3'$-plane. For each r_p-value there exists a limiting value of d^*_{min} beyond which no closed orbit exists. The limiting value of d^*_{min} for a sphere ($r_p = 1$) and a cylinder ($r_p = \infty$) calculated by Cox *et al.* (1968) are included in figure 3 as

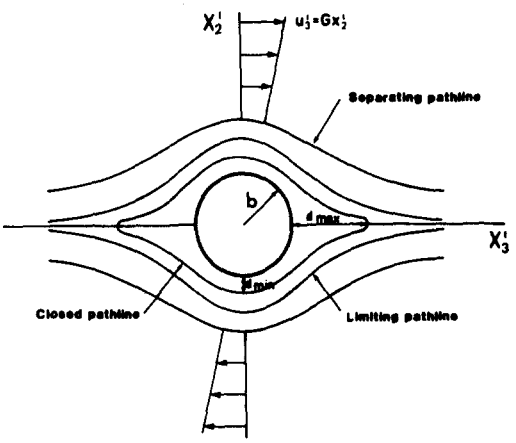

Figure 2. Pathlines (streamlines) around a sphere or spheroid oriented at $\theta = 0°$ (schematic). Two types of pathline exist: open separating ones and closed ones, separated by a limiting pathline. The minimum and maximum distance of a closed orbit to the surface of the spheroid are denoted by d_{min} and d_{max} respectively.

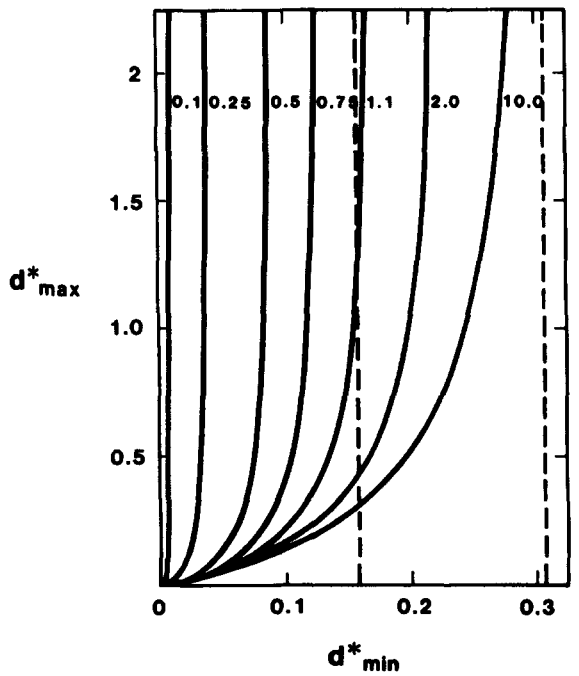

Figure 3. Values of d^*_{min} and d^*_{max} for closed orbits in the equatorial plane for various particle axis ratio's r_p. The dashed lines denote the asymptotic values of d^*_{min} for spheres and cylinders respectively, calculated by Cox *et al.* (1968).

indicated by the dashed lines. Each curve in figure 3 tends asymptotically to infinity at some limiting value of d^*_{min}. These limiting values of d^*_{min} are the minimum distances of approach of a small particle approaching from infinity (in the absence of interparticle forces or Brownian motion). At values larger than the limiting value of d^*_{min} only open pathlines exist.

For a cylinder of infinite length ($r_p = \infty$) the orbits are independent of x_1', i.e. independent of how far a particle is removed from the equatorial plane $X_2'X_3'$. For a spheroid of finite length the values of d_{min} and d_{max} depend on x_1'. Figure 4 shows various cross sections of spheroids

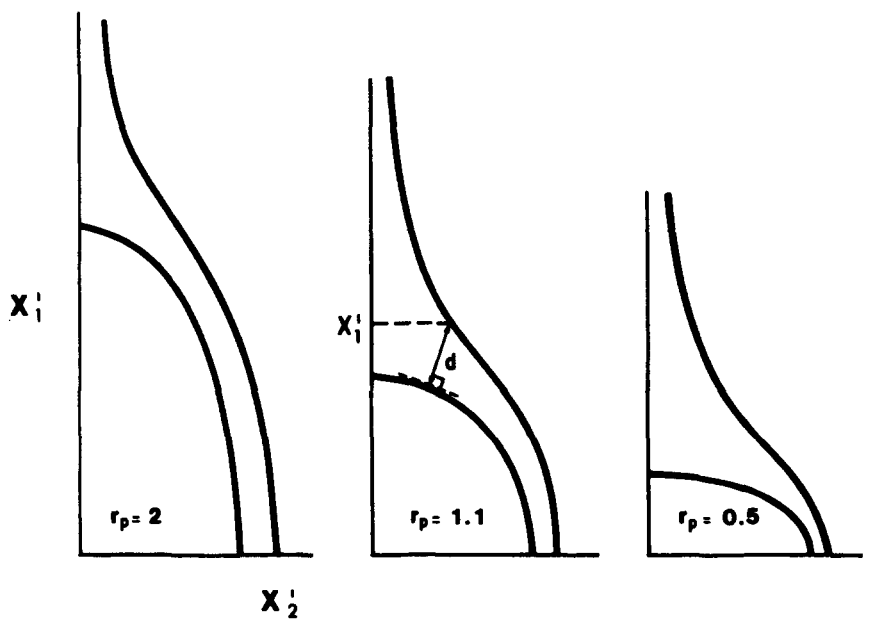

Figure 4. Cross sections of various spheroids aligned along the vorticity axis X_1', together with the curves separating the regions from open and closed pathlines. It shows that once r_p decreases the region of closed orbits gets larger. The distance between the limiting pathline at a given value of x_1' and the surface of the spheroid is denoted by d.

together with the curve which separates the open from the closed pathlines (in the $X_1'X_2'$ plane). It can be seen that for disk-shaped bodies the volume of closed pathlines above the particle is relatively much larger than for prolate spheroids. This has direct implications to problems of mass or heat transfer to (or from) such particles since in the region where closed pathlines exist the convective contribution is expected to be negligible. Consequently the local transfer rates decrease significantly and are mainly controlled by conduction or diffusion through the region of closed pathlines. Because the extension of the region where the rotational motion of fluid occurs increases linearly with the size of the spheroidal particle, it is easy to predict that the transfer rates will decrease as the object becomes larger.

For disks and rods of small r_p, the minimum distance between the spheroid and the surface separating open from closed orbits is always in the $X_2'X_3'$-plane. For prolate spheroids with larger r_p, this is no longer the case as is evident from figure 5. Here the distance d between limiting pathlines and the surface of the spheroid is shown as a function of x_1'/a. As can be seen from figure 2, the minimum distance between a pathline and the spheroid always occurs when $x_3' = 0$. The definition of d is shown in figure 4 for $r_p = 1.1$ where d is shown for a given value x_1'. It can be seen that for $r_p < 2$, $d^*(= d/b)$ always increases with x_1'; however at higher r_p a minimum appears near the top of the spheroid ($x_1'/a = 1$). This result is relevant to studies in orthokinetic coagulation. It is known from the study of two sphere interactions in shear flow, that the minimum distance of approach d^*_{min} is a very important parameter; if d^*_{min} is small, particles can approach to within distances over which colloidal forces are acting and coagulation might result; if d^*_{min} is large, the particles pass each other at distances where colloidal forces are negligible. It seems logical to assume that the efficiency with which fibers (prolate spheroids), oriented at $\theta = 0°$, can capture small particles is larger at positions where d_{min} is minimum, i.e. at the center of the fiber when $r_p \leqslant 5$ and at the ends of the fiber when $r_p \geqslant 5$. However it should be remembered that the number of collisions near the center is always larger than near the ends because x_2' and thus the velocity is larger.

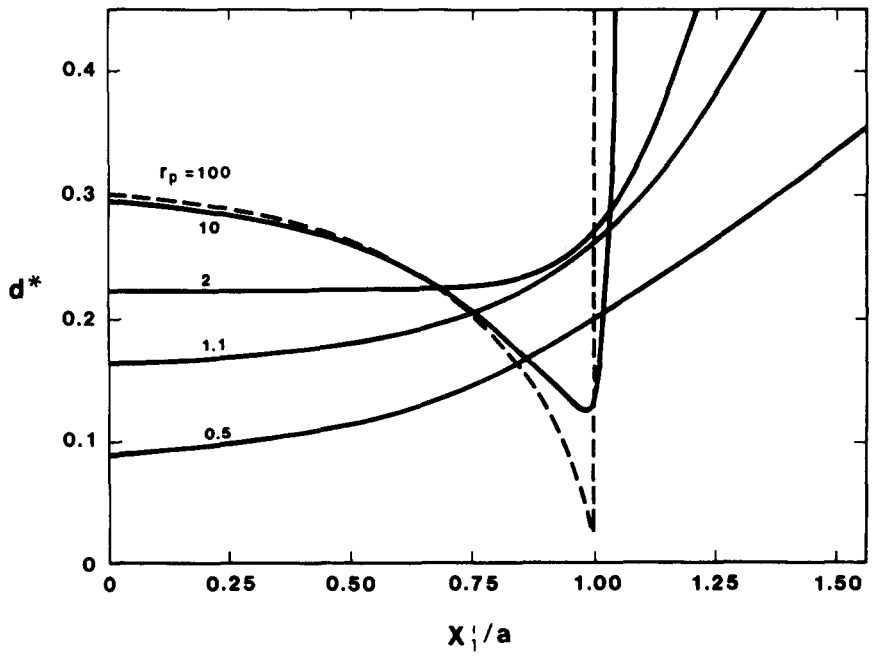

Figure 5. The distance $d^*(= d/b)$ between limiting pathlines and the surface of the spheroid as a function of x_1' for various $r_p(\theta = 0°)$. For small r_p the minimum distance occurs at $x_1' = 0$, i.e. at the center of the spheroid and at large r_p near $x_1' = a$, i.e. near the end.

(b) *Spheroids arbitrarily oriented*

Pathlines for spheroids not aligned along the vorticity-axis ($0° < \theta \leqslant 90°$) are often very different from those when $\theta = 0°$. We will distinguish two main types of pathline, each of which can be divided into two subclasses. The two main kinds are: (a) open pathlines, characterized by the feature that they approach from infinity, encounter the spheroid for a limited amount of time and separate towards infinity, and (b) permanent orbits which never wander off towards infinity. The open pathlines can be divided into two kinds: open single pass pathlines and transient orbits. The permanent orbits can be divided into closed and non-closed orbits. We will discuss these four kinds of pathline in some detail.

(i) *Single pass pathlines.* They are, of course, the rule when the initial value of x_2' or x_1' is large, similar to the open separating pathlines for spheres and spheroids oriented at $\theta = 0°$, in which case the open pathlines are symmetric about the X_2'-axis. In contrast, the pathlines passing by a spheroid rotating with a non-zero orbit constant (i.e. $0° < \theta \leqslant 90°$) are usually not symmetric. It is even possible for single pass pathlines to have a loop in their trajectory, without orbiting the spheroid.

(ii) *Transient orbits.* The possibility exists that a small particle arriving from infinity orbits the central spheroid n or $n + 1/2$ times and subsequently separates either in the same or in the opposite direction from which it came. Two examples of transient orbits are shown in figures 6(a) and (b) for $r_p = 2$ and $\theta = 90°$. This type of interaction is impossible for two sphere encounters. It is of interest to note that when the pathline disappears in the same direction from which it came, the pathline is always symmetric about the X_3'-axis (or more generally, the $X_1'X_3'$-plane). It can be seen from the geometry of the flow that pathlines obtained by forward integration starting from (x_1', x_2', x_3') and pathlines obtained by backward integration (in time) starting from $(x_1', -x_2', x_3')$ are mirror images, reflected in the $X_1'X_3'$-plane. If a pathline cuts this plane an odd number of times, the pathline and its mirror image are the same. Pathlines

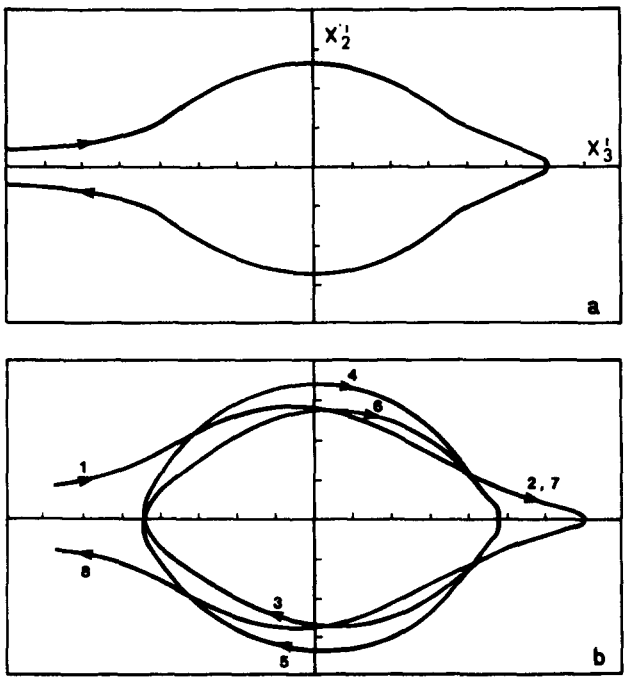

Figure 6. Examples of transient orbits in the equatorial plane ($\theta = 90°$) for spheroids of axis ratio $r_p = 2$, initially aligned along the X_2'-axis ($\phi_0 = 0$). (a) initial conditions: $x_1' = x_2' = 0$, $x_3'/b = 3$ (path of approach and recession from x_3' is symmetric). (b) initial conditions: $x_1' = 0$, $x_2'/b = 0.426$, $x_3'/b = -3.238$. The numbers indicate the course the pathline takes while orbiting the spheroid. For region 2, 7 the positions differ by less than the thickness of the line. Notice that here also the pathline is symmetric about the X_3'-axis. One division on the axis corresponds to $b/2$.

disappearing in the opposite direction from which they came cut the plane $X_1'X_3'$ an even number of times.

(iii) *Closed orbits.* A closed orbit is possible when a fluid element (or small particle) arrives at exactly the same position after n orbits, while in the same time the spheroid executes $(m+1)/2$ rotations ($m, n = 1, 2, 3$, etc.). When $n = m = 1$ there are two distinct possibilities: (a) the fluid element is at the surface of the spheroid and makes an orbit of period $T = 2\pi(r_p + r_p^{-1})/G$ which is closed when $\theta = 90°$; (b) there exists another closed orbit of period T shown in figure 7 for $r_p = 2$, $\theta = 90°$. Here the fluid element always stays at the same side of the spheroid. Initially when the fluid element is at $x_3' = 1.38b$ the spheroid, oriented along the X_2'-axis, rotates faster than the fluid element; when the spheroid has reached $\phi = \pi/2$, its angular velocity has slowed down, but the velocity of the fluid element has increased because x_2' is now larger. Hence the relative velocity between the fluid element and the spheroid is periodically increasing and decreasing. For one specific initial position (when $r_p = 2$: $x_3' = 1.38b$, $x_2' = 0$) these increases and decreases just cancel each other and the orbit is closed.

The existence of additional closed orbits is difficult to establish numerically: it is usually impossible to decide if an initial position is reached again exactly or approximately after n orbits around the spheroid. For some trivial pathlines it is possible to prove that closed orbits other than $n = m = 1$ exist, which suggests that others may exist as well. Consider a point at the surface of a spheroid oriented at θ-angles other than 0° and 90°. While the spheroid rotates with a period T about the vorticity axis X_1', the spheroid also spins around its axis of revolution with angular velocity

$$\omega_1 \equiv \frac{d\gamma}{dt} = \frac{1}{2} G \cos\theta. \qquad [10]$$

The pathline which the point at the surface describes in space will be closed if, after n rotations of the spheroid, the spheroid has made exactly m spins (m and n integers). For example, when $\phi_0 = 0$ and $r_p < 1$, then after n rotations of the (oblate) spheroid about the vorticity axis, integration of [10] using [4] yields

$$\gamma = cK(k)n \qquad [11]$$

where

$$c = \frac{2(r_p^2 + 1)}{r_p(C^2 + 1)^{1/2}},$$

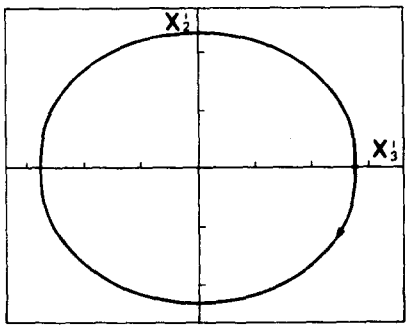

Figure 7. Example of closed orbit of period equal to the period of rotation of the spheroid. Axis ratio $r_p = 2$, $\theta = 90°$. The fluid element always stays at the same side of the spheroid. Initial conditions: $\phi_0 = 0$, $x_2' = 0$, $x_3'/b = 1.38$.

C being the orbit constant (i.e. the value of $\tan\theta$ at $t=0$); $K(k)$ is the complete elliptical integral of the first kind of modulus k, where

$$k = C\sqrt{[(1-r_p^2)/(C^2+1)]}.$$

For the spheroid to execute exactly m spins during n rotations we have

$$2\pi m = cK(k)n$$

or [12]

$$m/n = \tilde{c}$$

where $\tilde{c} = cK/2\pi$.

A similar integration can be performed when $r_p > 1$ (Anczurowski & Mason 1967). For a spheroid with a given value of r_p, there exist certain values of C for which $\tilde{c}$ is a rational number and other values for which $\tilde{c}$ is irrational. In the former case a solution of [12] exists and hence the pathline of the point at the surface becomes closed after n rotations of the spheroid. In the latter case [12] has no solutions and the pathline is not closed, although for sufficiently large values of m and n the pathline will return arbitrarily close to its initial position (an infinite number of times). Such orbits, which are not closed but are contained within a finite volume of space, we will call permanent non-closed orbits.

The question whether there are more closed than non-closed permanent orbits boils down to whether there are more rational than irrational numbers. Because there are infinitely more irrational than rational numbers (see e.g. Ogilvy & Anderson 1966), non-closed orbits are the rule and closed orbits the exception. The latter ones are probably isolated ones and do not contribute to the volume of liquid around the spheroid. This is rather different from the streamlines around a sphere (in an infinite medium) for which the volume of closed orbits is infinite.

(iv) *Permanent non-closed orbits.* From our numerical calculations we found that in some cases pathlines continued to orbit the central spheroid apparently without any tendency to move closer or further away (on the average) sometimes for up to several hundred rotations.

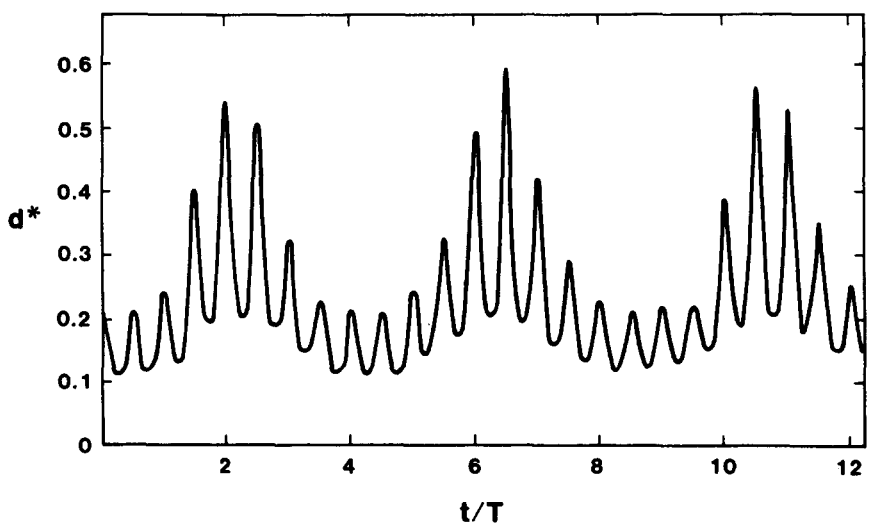

Figure 8. Apparently permanent non-closed orbits in the equatorial plane ($\theta = 90°$) for spheroids of axis ratio $r_p = 2$. Plotted is the distance between the position of the fluid element and the surface of the spheroid while in orbit around it, as a function of time. Initial conditions: $\phi_0 = 0$, $x_1' = x_2' = 0$, $x_3'/b = 1.21$.

However their orbits were not closed but every one of them was different. This suggests that those orbits are permanent non-closed orbits similar to the trivial ones described above. Some of them might become closed after a larger number of orbits and others might be degenerate cases of pathlines of type (ii), i.e. they could conceivably separate after many orbits. An example of such apparently non-closed orbits is given in figure 8 for $r_p = 2$, $\theta = 90°$, $\phi_0 = 0°$, $x_1' = x_2' = 0$, $x_3'/b = 1.21$, where the distance (non-dimensionalized by b) between the position of the fluid element and the surface of the spheroid is shown as a function of time (non-dimensionalized by the period of rotation of the spheroid). Although the variation in distance shows regularities, it can clearly be seen that each orbit is different. Such orbits resemble the changes in θ for a triaxial ellipsoid in shear (Harris *et al.* 1979).

Pathlines which permanently orbit the spheroid are always contained within a finite amount of volume. This is evident from figure 9 where a permanent orbit similar to the one in figure 8 is shown in particle fixed coordinates. It can be clearly seen that the pathlines are contained within a finite volume; for the case shown in figure 9 this volume rotates along with the spheroid. Again such regions are important with respect to heat (or mass) transfer from such particles, as heat cannot be convected away from such places. Probably such regions of permanent orbits contain both non-closed and closed orbits, similar to pathlines at the spheroid's surface.

After having described the possible pathlines around freely rotating spheroids, we now focus our attention on when and where they occur. When θ is close to zero or r_p close to one, most orbits which were previously (i.e. for $\theta = 0$ or $r_p = 1$) closed now become permanently non-closed (or closed after large n), with each cycle nearly closed. Most open separating pathlines which were previously symmetric become slightly asymmetric. The surface of limiting streamlines is replaced by a very narrow region of transient orbits.

In essence the same is true for other values of r_p and θ, except that the permanent orbits become more irregular and the single pass pathlines more asymmetric. An example is given in figure 10 for $\theta_0 = 30°$ and $r_p = 2$. The figure shows the transition region of transient orbits, with the number of orbits N it takes to separate as a function of initial distance d to the spheroid (in

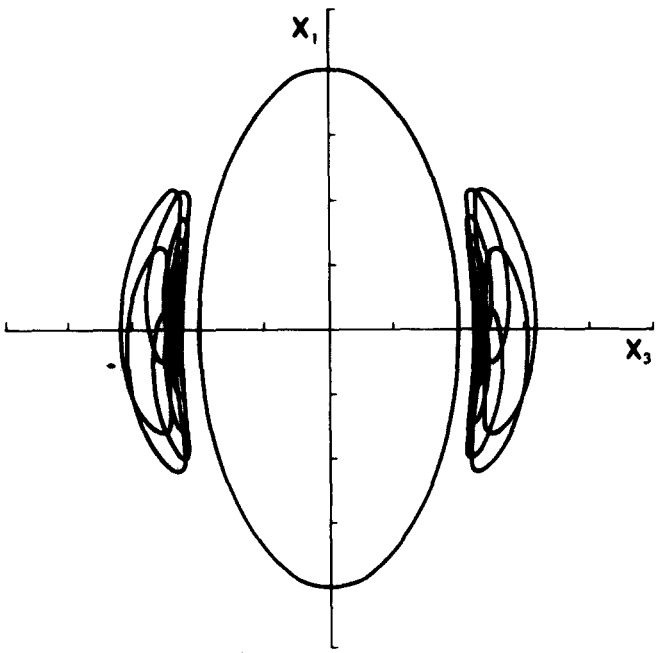

Figure 9. Regions of permanent non-closed orbits, rotating along with the spheroid, shown in particle-fixed coordinate system. The initial orientation of the spheroid of $r_p = 2$ was $\theta = 90°$, $\phi_0 = 0°$. Calculations of pathlines were started at $x_3/b = 1.2$.

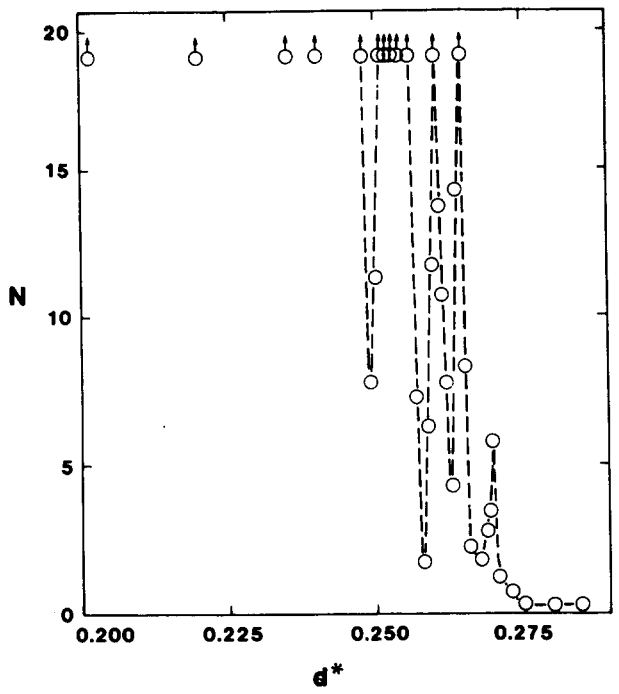

Figure 10. Example of transition region consisting of transient orbits for spheroid of $r_p = 2$ with initial orientation $\theta = 30°$, $\phi_0 = 0°$. Plotted are the number of orbits before separating towards infinity, N, as a function of the initial distance d (non-dimensionalized by b; $d^* = d/b$) from the surface. The distance d is taken along the X_2-axis which initially lies in the $X_1'X_2'$-plane. $N = 1/4 + n$ (n being a positive integer) denotes the case of a pathline going to infinity in the positive X_3'-direction. $N = 3/4 + n$ denotes the case when the pathline disappears in the opposite direction.

the X_2-direction, i.e. the initial positions are located in the $X_1'X_2'$-plane a distance d from the spheroid). It can be seen that for $d^* > 0.275$ the pathline separates immediately towards infinity. The data seem to suggest that the number of orbits before separating approaches a large value at $d_0^* \simeq 0.245$. Unfortunately, due to computer time limitations and numerical round-off errors, it is not possible to prove that some value of $d, N \to \infty$; nevertheless the fluid element trajectories for $d_0^* < 0.245$ were followed in these series of calculations for up to 50 rotations, with no apparent tendency to move away from the rotating spheroid. This suggests that at $d^* < d_0^*$ orbits of type (iv) exist. At $d_0^* < d^* < 0.275$ transient orbits exist. The transition region is rather irregular as seen from the numerous maxima and minima in the curve. This may be related to differences in relative velocities of fluid elements and spheroids as d changes.

Hence qualitatively the situation shows similarities with the streamlines around spheres. There we have permanent orbits (closed ones) and open streamlines, separated by a surface of limiting streamlines. The pathlines around spheroids at $\theta \neq 0°$ consist of permanent orbits (probably mainly non-closed with isolated closed ones) and open (single pass) pathlines, separated by a region of transient orbits. However the various regions are not as well-defined as in the case of spheres. Their extension depends on the orientation of the spheroid. All types of pathline can pass through the same region of space at different times.

The existence of permanent orbits around rotating spheroids in the case where $\theta > 0°$ within a relatively large region (extending up to 30% of the particle radius) has important implications for the prediction of mass and heat transfer rates. Analogous to the previously discussed case of $\theta = 0°$, the mechanism of mass (or heat) transfer through the region of circulating fluid (permanent orbits) will mainly consist of diffusion (or conduction) with little contribution of convection effects. As a result, the mass (or heat) transfer rates are expected to be considerably reduced (as compared to a stationary spheroid in a shear flow), especially for larger spheroidal

particles and low diffusion coefficients (conductivities) which is the case e.g. for deposition of colloidal particles on cellulose fibers.

4. CONCLUDING REMARKS

From the data presented above it can be seen that the pathlines around rotating oblate or prolate spheroids follow, in general, a rather complicated course. We have identified four different types of pathline, although this classification is somewhat arbitrary. For example, open (single pass) pathlines containing loops could in some instances be rather similar to transient orbits; this depends on how big such a loop must be before it can be considered to orbit the spheroid. Numerically it is hard to differentiate between permanent non-closed orbits, closed orbits (of large n) and transient orbits which separate after many orbits, because the amount of computer time becomes prohibitive and the occurrence of small accumulative errors as $t^* \to \infty$. The question whether permanent orbits are non-closed or closed after many orbits is rather academic; they can apparently be non-closed for several hundred rotations, which is usually much longer than time scales relevant to practical applications or experimental verifications. Despite the problems associated with our classification, the distinctions made between various pathlines are useful and provide insights into the possible courses pathlines can take.

It can be expected that small particles (of radius $< 0.1b$) will follow the pathlines rather accurately, provided colloidal forces between the particle and the spheroid are absent. At present we are extending our calculations to systems in which colloidal forces between the particle are acting, in order to study the problem of deposition of small particles on disks and rods rotating in shear flow. This will be described in a forthcoming publication.

It is possible that trajectories of spheres of size comparable to the minor axis of the spheroid are qualitatively similar to the pathlines described above, analogous to the qualitative similarity between streamlines around single spheres and relative trajectories between equal or unequal-sized spheres. For instance, using the traveling microtube technique (Vadas *et al.* 1973), we have observed a transient orbit of the type shown in figure 6(a) for the case of a 4 μm dia. polystyrene latex sphere making one orbit around a doublet consisting of two such spheres, flowing through a capillary tube of about 200 μm dia. This could mean that, here too, we have permanent orbits and single pass trajectories, separated by a region of transient orbits.

It follows from some of our remarks made above that the description of pathlines around spheroids is relevant to problems of heat and mass transfer in flowing suspensions of spheroidal particles, including the problems related to the deposition of small particles on spheroids subjected to shear. It also is a prerequisite for understanding the relative motion of more irregularly shaped bodies in simple shear.

Acknowledgement—The authors wish to thank Dr. S. G. Mason for his stimulating interest in this research.

REFERENCES

ADLER, P. M. 1981 Interactions of unequal spheres. I. Hydrodynamic interactions, colloidal forces. *J. Colloid Interface Sci.* **84**, 461–474.

ANCZUROWSKI, E. & MASON, S. G. 1967 The kinetics of flowing dispersions. II. The equilibrium orientations of rods and discs (theoretical). *J. Colloid Interface Sci.* **23**, 522–546.

ARP, P. A. & MASON, S. G. 1977 The kinetics of flowing dispersions. VIII. Doublets of rigid spheres (theoretical). *J. Colloid Interface Sci.* **61**, 21–43.

HARRIS, J. B., NAWAZ, N. & PITTMAN, J. F. T. 1979 Low Reynolds-number motion of particles with two or three perpendicular planes of symmetry. *J. Fluid Mech.* **95**, 415–429.

BATCHELOR, G. K. & GREEN, J. T. 1972 The hydrodynamic interactions of two small freely moving spheres in a linear flow field. *J. Fluid Mech.* **56**, 375–400.

COX, R. G., ZIA, I. Y. Z. & MASON, S. G., 1968. Particle motion in sheared suspensions. XXV. Streamlines around cylinders and spheres. *J. Colloid Interface Sci.* **27**, 7–18.

BATCHELOR, G. K. 1967 *An Introduction to Fluid Dynamics.* Cambridge University Press, p. 139.

JEFFERY, G. B., 1922 The motion of ellipsoidal particles immersed in a viscous fluid. *Proc. Roy. Soc.* **A102**, 161–179.

OGILVY, C. S. & ANDERSON, J. T. 1966 *Excursions in Number Theory.* Oxford University Press, New York, Chap. 6.

VADAS, E. G. GOLDSMITH, H. L. & MASON, S. G. 1973 The microrheology of colloidal dispersions. I. The microtube technique. *J. Colloid Interface Sci.* **43**, 630–648.

VAN DE VEN, T. G. M., 1982 Interactions between colloidal particles in simple shear flow. *Advances Colloid Interface Sci.* **17**, 105–127.

APPENDIX I

Flow field near spheroid

By setting $c = b$ in Jeffery's equations (22)–(24) (Jeffery 1922) one obtains:

$$u_1^J = x_1\{\alpha_{21}\alpha_{31} + \beta'(W - V) - 2(\alpha + 2\beta)A\}$$

$$+ x_2\{\alpha_{22}\alpha_{31} + \beta' T^* - 2(\beta - \alpha)H\}$$

$$+ x_3\{\alpha_{23}\alpha_{31} + \beta' S - 2(\beta - \alpha)G^*\}$$

$$-\frac{2x_1P^2}{(a^2+\lambda)\Delta}\left[\tilde{R} + \frac{x_2^2\tilde{W}}{(b^2+\lambda)^2} - \frac{x_3^2\tilde{V}}{(b^2+\lambda)^2}\right] \qquad [1a]$$

$$u_2^J = x_1\{\alpha_{21}\alpha_{32} + \beta' T^* + 2(\beta - \alpha)H\}$$

$$+ x_2\{\alpha_{22}\alpha_{32} + \alpha' U - \beta' W - 2(\alpha + 2\beta)B^*\}$$

$$+ x_3\{\alpha_{23}\alpha_{32} + \alpha' R\}$$

$$-\frac{2x_2P^2}{(b^2+\lambda)\Delta}\left[\tilde{R} - \frac{x_1^2\tilde{W}}{(a^2+\lambda)^2} + \frac{x_3^2\tilde{U}}{(b^2+\lambda)^2}\right] \qquad [1b]$$

$$u_3^J = x_1\{\alpha_{21}\alpha_{33} + \beta' S - 2(\alpha - \beta)G^*\}$$

$$+ x_2\{\alpha_{22}\alpha_{33} + \alpha' R\}$$

$$+ x_3\{\alpha_{23}\alpha_{33} + \beta' V - \alpha' U - 2(\alpha + 2\beta)C^*\}$$

$$-\frac{2x_3P^2}{(b^2+\lambda)\Delta}\left[\tilde{R} + \frac{x_1^2\tilde{V}}{(a^2+\lambda)^2} - \frac{x_2^2\tilde{U}}{(b^2+\lambda)^2}\right]. \qquad [1c]$$

Here

$$A = \frac{\alpha_{21}\alpha_{31}}{6\beta_0}$$

$$B^* = \frac{\beta_0''(2\alpha_{22}\alpha_{32} - \alpha_{23}\alpha_{33}) - \alpha_0''\alpha_{21}\alpha_{31}}{6\beta_0''(2\alpha_0'' + \beta_0'')}$$

$$C^* = -(A + B^*)$$

$$F = \frac{\alpha_{22}\alpha_{33} + \alpha_{23}\alpha_{32}}{8\alpha_0' b^2}$$

$$G^* = \frac{\alpha_{23}\alpha_{31} + \alpha_{21}\alpha_{31}}{4\beta_0'(a^2 + b^2)}$$

$$H = \frac{\alpha_{21}\alpha_{32} + \alpha_{22}\alpha_{31}}{4\beta_0'(a^2 + b^2)}$$

$$R = -4Fb^2 \qquad U = 2(B^* - C^*)b^2$$

$$S = 2G^*(a^2 + b^2) \qquad V = 2(b^2 C^* - a^2 A)$$

$$T^* = -2H(a^2 + b^2) \qquad W = -(U + V)$$

$$\tilde{R} = \frac{x_2 x_3}{(b^2 + \lambda)^2}\{R + 4(b^2 + \lambda)F\} + \frac{x_1 x_3}{(a^2 + \lambda)(b^2 + \lambda)}\{S + 2(a^2 + b^2 + 2\lambda)G^*\}$$

$$+ \frac{x_1 x_2}{(a^2 + \lambda)(b^2 + \lambda)}\{T^* + 2(a^2 + b^2 + 2\lambda)H\}$$

$$\tilde{U} = U - 2(b^2 + \lambda)(B^* - C^*)$$

$$\tilde{V} = V - 2(b^2 + \lambda)C^* + 2(a^2 + \lambda)A$$

$$\tilde{W} = W - 2(a^2 + \lambda)A + 2(b^2 + \lambda)B^*.$$

Also,

$$\frac{1}{P^2} = \frac{x_1^2}{(a^2 + \lambda)^2} + \frac{x_2^2 + x_3^2}{(b^2 + \lambda)^2}.$$

$$\Delta = (b^2 + \lambda)(a^2 + \lambda)^{1/2},$$

λ is the positive root of $\frac{x_1^2}{a^2 + \lambda} + \frac{x_2^2 + x_3^2}{b^2 + \lambda} = 1.$

Moreover:

$$\alpha = \int_\lambda^\infty \frac{d\lambda}{(a^2 + \lambda)\Delta} = p - \frac{2}{s^2(a^2 + \lambda)^{1/2}}$$

where

$$p = \frac{1}{s^3}\left\{\tan^{-1}\frac{(a^2 + \lambda)^{1/2}}{s} + \frac{\pi}{2}\right\} \quad \text{if } r_p = \frac{a}{b} < 1$$

$$= \frac{1}{s^3}\ln\frac{(a^2 + \lambda)^{1/2} + s}{(a^2 + \lambda)^{1/2} - s} \quad \text{if } r_p > 1$$

with

$$s^2 = |a^2 - b^2|.$$

$$\beta = \int_\lambda^\infty \frac{d\lambda}{(b^2+\lambda)\Delta} = \frac{1}{(b^2+\lambda)(a^2+\lambda)^{1/2}} - \frac{\alpha}{2}$$

$$\alpha' = \int_\lambda^\infty \frac{d\lambda}{(b^2+\lambda)^2\Delta} = \frac{(a^2+\lambda)^{1/2}}{2s^2(b^2+\lambda)^2} - \frac{3\beta}{4s^2}$$

$$\beta' = \int_\lambda^\infty \frac{d\lambda}{(a^2+\lambda)(b^2+\lambda)\Delta} = \frac{\beta-\alpha}{s^2}$$

$$\alpha'' = \int_\lambda^\infty \frac{\lambda\, d\lambda}{(b^2+\lambda)^2\Delta} = \beta - \alpha'$$

$$\beta'' = \int_\lambda^\infty \frac{\lambda\, d\lambda}{(a^2+\lambda)(b^2+\lambda)\Delta} = \alpha - \beta'.$$

The corresponding integrals with the lower limit of integration replaced by zero are denoted by α_0, α_0', α_0'', β_0, β_0' and β_0''.